

**$^{59}\text{Co}$  NMR study of the allotropic phase transformation in small ferromagnetic cobalt particles**R. Speight,<sup>1</sup> A. Wong,<sup>1</sup> P. Ellis,<sup>2</sup> P. T. Bishop,<sup>2</sup> T. I. Hyde,<sup>2</sup> T. J. Bastow,<sup>3</sup> and M. E. Smith<sup>1,\*</sup><sup>1</sup>*Department of Physics, University of Warwick, Coventry CV4 7AL, United Kingdom*<sup>2</sup>*Johnson Matthey Technology Centre, Blounts Court, Sonning Common, Reading RG4 9NH, United Kingdom*<sup>3</sup>*Division of Materials Science and Engineering, CSIRO, Private Bag 33, Clayton, Victoria 3169, Australia*

(Received 2 August 2008; revised manuscript received 23 November 2008; published 4 February 2009)

To demonstrate the potential of nuclear-magnetic-resonance (NMR) spectroscopy in investigating detailed structural properties in ferromagnetic materials, the allotropic phase transformation of polycrystalline cobalt with  $\mu\text{m}$  particle size ( $<2 \mu\text{m}$ ) is characterized by internal-field  $^{59}\text{Co}$  NMR. The  $^{59}\text{Co}$  NMR spectra show distinct resonance bands corresponding to the different Co sites: face-centered cubic (fcc), hexagonal-close packed (hcp), and stacking faults (sfs), in Co metal powder. The hcp $\rightarrow$ fcc phase-transition temperature is determined by systematically monitoring the signal intensity of each Co environment in a series of heat-treated Co powders. The potential limits to which absolute quantification of the different sites can be pushed are mentioned, with relative changes in intensity giving unequivocal evidence of the structural evolution. For example, the phase-transition temperature is observed to be  $500 \pm 25 \text{ }^\circ\text{C}$ , and above this temperature, the sf Co sites were reduced by more than 10%.

DOI: [10.1103/PhysRevB.79.054102](https://doi.org/10.1103/PhysRevB.79.054102)

PACS number(s): 61.72.Hh, 61.05.Qr, 82.56.Ub

**I. INTRODUCTION**

The allotropic phase transformation from the hexagonal-close-packed (hcp) phase to the face-centered-cubic (fcc) phase of bulk cobalt (Co),  $\text{fcc} \xrightleftharpoons[\text{heating}]{\text{cooling}} \text{hcp}$ , has been studied by x-ray diffraction (XRD),<sup>1</sup> electron diffraction,<sup>2</sup> acoustic measurements,<sup>3</sup> and by theoretical calculation.<sup>4</sup> From XRD, the phase-transition temperature was found to be at  $417 \text{ }^\circ\text{C}$ , with considerable hysteresis between  $390\text{--}430 \text{ }^\circ\text{C}$ .<sup>1</sup> However, Kitakami *et al.*<sup>5</sup> have reported that there is a close relationship between the Co crystallite size and the crystal phase. In general at room temperature, hcp is the dominant phase for Co crystallites with diameter ( $d$ )  $>40 \text{ nm}$ , fcc phase for  $d \leq 20 \text{ nm}$ , and a mixture of hcp and fcc phases for  $d$  in the range of  $20\text{--}40 \text{ nm}$ . Conventional XRD relies on long-range order; hence materials with crystallite size in the nanometer range are often difficult to detect quantitatively by XRD. Although structural information on stacking faults (sfs) can be obtained from XRD, models of particular crystal defects are difficult to verify from powder XRD data. Unlike XRD, nuclear magnetic resonance (NMR) is well suited to study the local structural environments around the Co site.<sup>6</sup> As  $^{59}\text{Co}$  (100% natural abundance, nuclear-spin  $7/2$ ) NMR spectra give distributions of hyperfine fields for all Co atoms,  $^{59}\text{Co}$  NMR spectra are sensitive to the change in Co occupancy and local environment (i.e., spin or electron distribution of Co, and different Co sites). Since cobalt is a ferromagnetic metal, conventional  $^{59}\text{Co}$  NMR cannot be applied. Internal field  $^{59}\text{Co}$  NMR of ferromagnetic Co was first observed in 1959 by Gossard and Portis,<sup>7</sup> and since then the application of internal-field NMR to ferromagnetic materials has developed considerably.<sup>8–10</sup> There has been an extensive subsequent use of  $^{59}\text{Co}$  NMR to characterize the different Co atomic environments [fcc, hcp, and sfs] in Co metal,<sup>11–15</sup> in Co films,<sup>16–19</sup> in catalysts,<sup>20,21</sup> and in alloys.<sup>22–26</sup> However, the allotropic phase transformation of small Co particles has never been investigated by NMR spectroscopy.

Here the allotropic phase transformation of a ferromagnetic material is characterized by solid-state NMR spectroscopy. The allotropic (hcp $\rightarrow$ fcc) phase-transition temperature of Co with small particle size ( $<2 \mu\text{m}$ ) is determined by monitoring the behavior of the different Co sites after heating and subsequent quenching.

Since Gossard and Portis<sup>7</sup> first investigated internal-field  $^{59}\text{Co}$  NMR in  $20 \text{ nm}$  Co metal particles in a  $\gamma$ -alumina matrix and observed the resonance at  $213.1 \text{ MHz}$  for Co in the fcc phase, there have been a number of reports of the NMR assignments for the different Co sites. The assignments used in the current work are based on one of the more recent reports by Sort *et al.*:<sup>15</sup>  $213.1 \text{ MHz}$ —unfaulted fcc,  $221.0 \text{ MHz}$ —unfaulted hcp,  $214.0$  and  $215.5 \text{ MHz}$ —one fcc twin fault, which can be classified as two consecutive hcp deformation sfs, and  $217.0$  and  $219.0 \text{ MHz}$ —one hcp twin fault, which can be classified as two consecutive fcc deformation sfs.

**II. NMR ANALYSIS**

Unlike nonmagnetic materials, NMR analysis of ferromagnetic materials requires extra care and attention. The observed NMR intensity in a ferromagnetic material does not directly correspond to the relative number of nuclei at any given frequency. This is due to the fact that the NMR applied rf field ( $h_1$ ) does not directly induce the NMR signal but instead  $h_1$  affects the oscillation of the internal hyperfine field ( $H_{\text{rf}}$ ), i.e., electronic magnetization, which has a transverse component ( $h_\perp$ ) that is responsible for the observed NMR signal. In such magnetic materials where the particles are made up of multiple magnetic domains, the major process generating the magnetic signal in response to the applied rf field is displacement of domain walls.<sup>8,10</sup> It is the nuclear spins within the magnetic domain walls that are effectively excited and generate the observed signal. Hence the distribution of the magnetic domain walls will have an effect on the spectrum recorded; but in a complex multiphase pow-

der sample such as this, the domain walls should sample all the different phases. The fact that signals from all the species expected to be present are observed and that there is good general agreement with the x-ray data provides some evidence as to the validity of this approach. Unlike normal NMR, some function of the applied  $h_1$  field is responsible for the NMR signal. This factor is termed the enhancement factor ( $\eta$ ).<sup>27</sup> Equation (1), taken from the work of Malinowska *et al.*,<sup>27</sup> clearly expresses the relationship between the observed NMR signal  $S(h_1, \omega)$  at a given frequency ( $\omega$ ) and effective applied rf field ( $h_1$ ), and the actual “corrected” signal intensity [ $I_0(\omega)$ ],

$$S(h_1, \omega) = \eta I_0(\omega) \exp[-\log^2(h_1/h_{1\text{opt}})/2\sigma^2], \quad (1)$$

where  $h_{1\text{opt}}$  is the rf field for which the observed NMR signal is maximum, also known as the optimum rf value, and  $\sigma$  is the width of the Gaussian distribution in  $\log(h_1)$ . Panissod *et al.* demonstrated that the  $^{59}\text{Co}$  NMR spectrum using  $I_0(\omega)$  from ferromagnetic Co can be acquired by plotting a two-dimensional (2D) signal intensity spectrum as a function of frequency ( $\omega$ ) and an applied rf field ( $h_1$ ). The projection in the frequency domain gives the maximum intensity measured in the 2D data set where  $h_1$  is  $h_{1\text{opt}}$ . Then Eq. (1) becomes  $S(h_{1\text{opt}}, \omega) = \eta I_0(\omega)$ . As  $S(h_{1\text{opt}}, \omega)$  is not a true representation of the actual intensity [ $I_0(\omega)$ ],  $S(h_{1\text{opt}}, \omega)$  must be divided by the dimensionless frequency-dependent enhancement factor ( $\eta$ ). Furthermore Panissod *et al.*<sup>28</sup> showed that  $1/\eta$  is proportional to  $h_{1\text{opt}}$ , (which is taken as a dimensionless number<sup>27</sup>) such that, to give the spectrum with the corrected signal intensity:  $I_0(\omega) \propto h_{1\text{opt}} \times S(h_{1\text{opt}}, \omega)$ .

### III. EXPERIMENTAL DETAILS

#### A. Co sample preparation

99.8% pure Co metal with a nominal particle size of 2  $\mu\text{m}$  and below was purchased from the Aldrich Chemical Co. (U.K.). Broadening of the XRD lines is consistent with this mean particle size, with electron microscopy indicating a fairly uniform powder with most particles in the 1–2  $\mu\text{m}$  range and very few particles outside this range (the one exception to this were the samples heated to 950  $^\circ\text{C}$  where fusing of particles increased their size up to 8  $\mu\text{m}$ ). The Co powder was heated to various treatment temperatures (200–950  $^\circ\text{C}$ ) at a rate of 3  $^\circ\text{C}$  per min in a platinum tube using a vertical Eurotherm furnace in an inert Argon atmosphere to prevent atmospheric oxidation. The Co powder was then held at the treatment temperature for 15 min before cooling. The cooling method is referred to as crash cooling (CC) as the heated sample is effectively quenched into liquid nitrogen. The number on the sample abbreviation, for example, CC200, indicates the treatment temperature, which is here 200  $^\circ\text{C}$ .

#### B. Solid-state $^{59}\text{Co}$ NMR

The  $^{59}\text{Co}$  NMR spectra were recorded on a Chemagnetics CMX Infinity spectrometer, which uses no external magnetic field, using a frequency-stepping method. For the 2D intensity spectrum, a series of NMR spectra were recorded at a

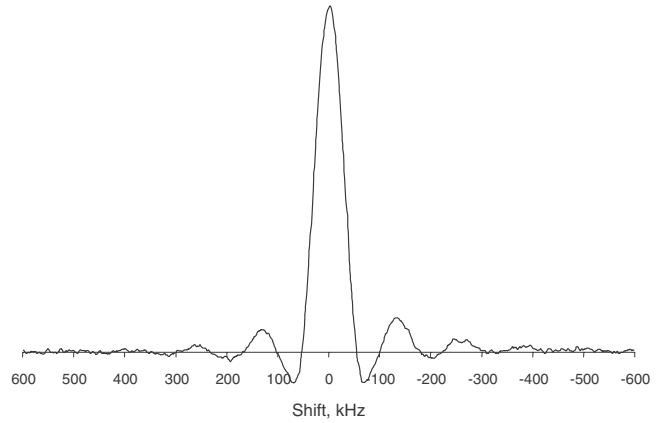


FIG. 1. A typical  $^{59}\text{Co}$  NMR spectrum formed by taking the Fourier transformation of the free induction decay (FID) measured from a spin echo of the untreated Co powder. It was taken at 213 MHz with  $h_1 = 5$  mT. Note that the shape is sinlike and this is due to the Fourier transform of the 10  $\mu\text{s}$  square  $180^\circ$  pulse. Furthermore the central peak crosses the  $x$  axis at  $\sim 52.5$  and  $-56.2$  kHz which corresponds to  $\sim 9.2$   $\mu\text{s}$ , which is close to the known  $180^\circ$  pulse length.

range of applied frequencies ( $\omega$ ) (210–228 MHz) with an increment of 100 kHz, and at a range of applied rf fields that produced effective rf fields in the sample of  $h_1$  (4–166 mT). For the majority of the work an NMR probe with a 9.5-mm-diameter coil was used as this produces a good signal to noise. A standard spin-echo experiment was carried out with 2000 scans and a pulse delay of 0.05 s. The effective “ $90^\circ$ ” pulse length (i.e., where a maximum signal was determined) was measured on the untreated metallic Co powder by varying the applied rf power. An interpulse delay of 20  $\mu\text{s}$  was used and no significant changes in the line shape was observed for either larger pulse or interpulse delays, indicating that these delays were optimized for all Co sites. The 2D  $^{59}\text{Co}$  NMR spectrum was built up by using the maximum point measured from NMR spectra taken at various frequencies and rf field strengths, and to get the full rf range a much smaller diameter (4 mm) probe was used. A typical spectrum is shown in Fig. 1 by Fourier transforming the echo. As discussed above the corrected signal intensity can be found from the 2D data set by taking the maximum intensity at every frequency (i.e., that of  $h_{1\text{opt}}$ ) multiplied by the dimensionless number proportional to  $h_{1\text{opt}}$ . From this corrected NMR spectrum Gaussian peaks were fitted to within 0.2 MHz of the literature values and the relative number of nuclei in each site is then equivalent to the relative areas under the Gaussians used to fit each site; the frequency was allowed to vary due to strain in the crystal lattice. DMFIT<sup>29</sup> was used for spectral fitting.

#### C. XRD

For comparison with NMR, powder XRD patterns were acquired for all Co powders using a Bruker AXS D8 diffractometer using a  $\text{Cu K}\alpha_1$  ( $\lambda = 1.5405$   $\text{\AA}$ ) x-ray source with a SolX energy dispersive detector. A relatively slow scanning speed was used (14 s/step, 0.022 $^\circ$  step size). The Co powder

was held in a stainless-steel holder and, as Co has a known absorption edge near Cu, a Ni filter was used. Rietveld refinement was used in an attempt to fit the XRD patterns to gain quantitative results on the relative Co site occupancy. This technique does not take into account crystal defects, i.e., sfs. Therefore for a full and more detailed analysis of the Co site occupancy, a more rigorous simulation would be necessary, as has been previously applied to platinum nanoparticles.<sup>30</sup> However as this is a difficult and time consuming exercise, it was decided that for the current work a comparison between the NMR and XRD results with Rietveld analysis would give a good first approximation.

#### IV. RESULTS AND DISCUSSION

##### A. <sup>59</sup>Co NMR data

Figure 2(a) shows the 2D <sup>59</sup>Co NMR spectrum,  $S(h_1, \omega)$ , of the untreated Co powder, and clearly illustrates the  $h_1$  and  $\omega$  dependences of the signal intensity. The maximum intensity for the different Co sites varies with both the rf strength and the observed frequency. For example, the  $h_{1opt}$  for the hcp site is found at 221.0 MHz with a rf of  $\sim 83$  mT, whereas 213.1 MHz and 125 mT are found for the fcc site. Figure 2(b) displays a projection spectrum in the frequency domain and is effectively  $S(h_{1opt}, \omega)$ , and hence is not a true representation of the correct NMR spectrum. As previously discussed, Panissod *et al.*<sup>28</sup> showed that  $S(h_{1opt}, \omega)$  is converted to the corrected NMR intensity by multiplying with the dimensionless number proportional to  $h_{1opt}$ , which is itself a function of frequency,<sup>27</sup> and the resultant corrected spectrum is shown in Fig. 3(a). The <sup>59</sup>Co NMR signal spreads over 13 MHz, from 210 to 223 MHz. The spectrum exhibits noticeable broad peaks at about 213, 215.5, and 221 MHz, indicating that there are multiple Co sites present in the Co powder. Spectral fitting with Gaussian line shapes reveals that there are a total of six bands, with linewidths in the range of 0.7–2.3 MHz. The observed broadening is attributed to a combination of the hyperfine interaction associated with the interaction between the nuclear spin and its own electron shell, and the local spin/electron distributions.<sup>7</sup> The frequency positions of the fitted bands are in good agreement with the previously reported <sup>59</sup>Co NMR studies by Gossard and Portis,<sup>7</sup> and Sort *et al.*<sup>15</sup> The <sup>59</sup>Co NMR results are summarized in Table I. Based on the spectral fitting, it was found that the untreated Co powder consists of  $20 \pm 3\%$  unfaulted fcc,  $52 \pm 3\%$  unfaulted hcp,  $10 \pm 3\%$  hcp deformation faults, and  $19 \pm 3\%$  fcc deformation faults. It should be noted that the errors quoted here are those deduced from the careful correction procedure adopted and the variation observed from multiple fitting of the data. However there are other factors that could produce systematic errors in the data such as the skin depth and domain-wall effects. It should be noted that the skin depth of Co at the rf frequencies used in the experiment is around  $8.6 \mu\text{m}$  and therefore has no problem penetrating the entire Co crystallite particle [ $d < 2 \mu\text{m}$  which was confirmed by scanning electron microscopy (SEM) and transmission electron microscopy (TEM)] used in this study. The domain walls are assumed to cover all the different components in these samples effec-

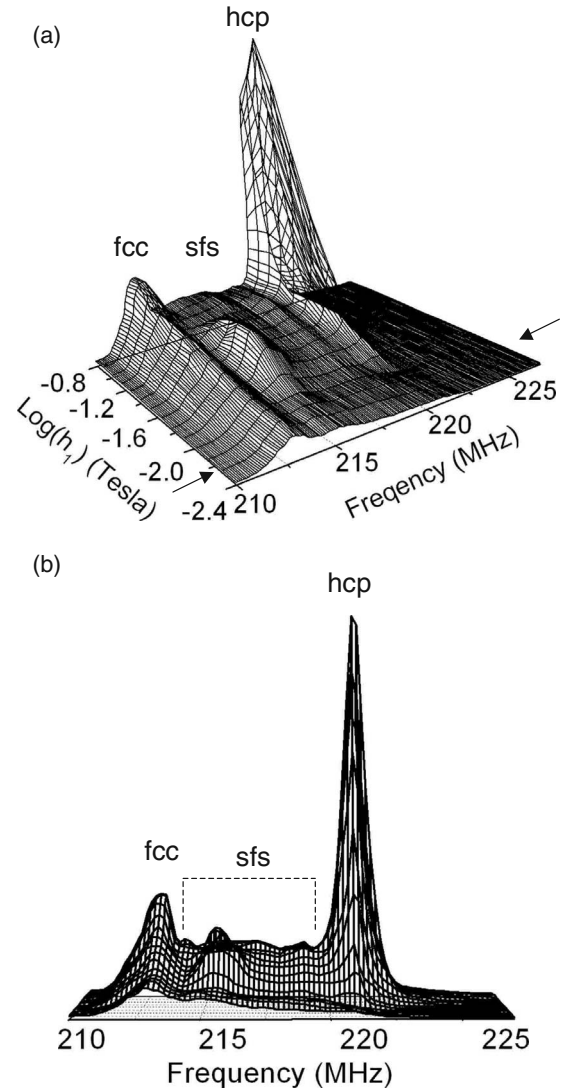


FIG. 2.  $S(h_1, \omega)$ , a 2D <sup>59</sup>Co NMR spectra of the untreated Co powder as a function of frequency,  $\omega$ , and rf field strength,  $h_1$ . Care was taken so that  $h_1$  was increased beyond the maximum measured intensity at each frequency. Panel (a) shows the data from an angle with arrows showing the rf field strength used in subsequent samples to take spectra. Panel (b) shows the observed frequency projection so that the maximum point at each frequency can be observed,  $S(h_{1opt}, \omega)$ .

tively and uniformly, i.e., not showing any significant bias, and the quantitative data presented later to some extent endorses this. Hence it is believed that the approach adopted here ensures reliable quantitative analysis. Even if this were not exactly true, the relative changes observed would allow the evolution of the sample to be followed qualitatively. In addition, the observed <sup>59</sup>Co NMR frequencies in Fig. 3(a) suggest that the Co particles produce a magnetic field ranging from 20.8 to 22.1 T [ $B = (v2\pi) / \gamma$ , where  $\gamma$  is the gyromagnetic ratio of Co,  $6.332 \times 10^7 \text{ rad T}^{-1} \text{ s}^{-1}$ , and  $v$  is the observed frequency].

It should be emphasized that the ability to probe the Co sfs (hcp/fcc deformation faults) in <sup>59</sup>Co NMR with ease is a great advantage over XRD. It is known that Rietveld analysis in XRD can be used to obtain quantitative information on the

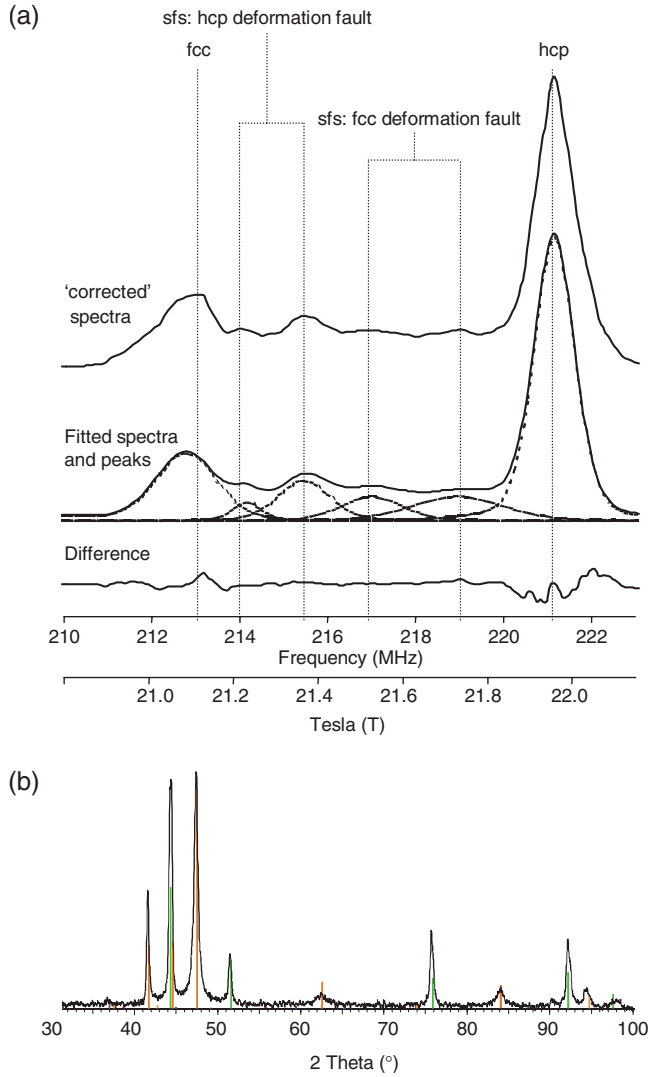


FIG. 3. (Color online) (a) Experimental and fitted corrected  $^{59}\text{Co}$  NMR spectra of the untreated Co powder. The vertical dotted lines show the positions of the different Co sites. (b) Experimental powder XRD pattern of the untreated Co powder, including the known angular positions for hcp (red bar, main peak 44.6), fcc (green bar, main peaks at 44.3, 51.7, 75.9, 92.2),  $\text{Co}_3\text{O}_4$  (blue bar, main peak (weak) 37.0), and CoO (orange bar, main peaks at 41.8, 47.6, 62.7, 84.1) (Refs. 32 and 33).

hcp-fcc content ratio and sfs.<sup>31</sup> However compared to XRD, NMR yields information on sfs in a more direct and straightforward way. Figure 3(b) shows a typical XRD pattern of the untreated Co powder, and shows that it detects the presence of both the hcp and fcc<sup>31,32</sup> phases as well as cobalt oxides ( $\text{Co}_3\text{O}_4$  and CoO). Careful fitting of the XRD pattern results in quantitative information from the metallic Co:  $24 \pm 5\%$  of fcc, and  $76 \pm 5\%$  of hcp. However the presence of sf phases has not been taken into account with this Rietveld fitting which may help in explaining the 15% difference in the phase content as deduced from fitting the NMR and XRD data. It has been suggested that the broadness of the peak at  $47.5^\circ$  ( $2\theta$ ) is attributed to strain in the sample, which is likely to be due to microtwin inclusion (sfs). However, the accuracy of any quantitative information on the sf phases gained by XRD is greatly reduced due to a combination of the small particle size and the structural disorder around such features.

As mentioned before, producing an NMR spectrum which is likely to represent the actual phase distribution for the untreated Co powder was acquired from a 2D intensity spectrum, which is somewhat time consuming. However the different Co sites in the heat-treated Co samples should exhibit the same enhancement factors, at all frequencies, as those in the untreated Co sample since the sites are the same between these different samples. Thus the signal intensity in an NMR spectrum for any given applied field [ $s(h_1 = \text{const}, \omega)$ ] is related to the  $S(h_{1\text{opt}}, \omega)$  spectrum by the same frequency-dependent conversion factor [ $C(\omega)$ ] as was deduced for each site in the nonheat-treated sample, such that

$$S(h_{1\text{opt}}, \omega) = C(\omega) \times s(h_1 = \text{const}, \omega), \quad (2)$$

where  $C(\omega)$  is the intensity ratio between the maximum signal, at  $h_{1\text{opt}}$  in Fig. 2(a), and the observed intensity at a given rf value,  $h_1$ . From the  $S(h_{1\text{opt}}, \omega)$  spectrum, the corrected NMR spectrum can be obtained by multiplying with the corresponding dimensionless number proportional to  $h_{1\text{opt}}$  at each given frequency. On this basis,  $^{59}\text{Co}$  NMR spectra for all of the heat-treated samples were recorded with an rf strength of  $h_1 = 5$  mT [indicated in Fig. 2(a) with arrows]. The resulting intensities are then multiplied by  $C(\omega)$ , the signal intensity ratio between rf field at  $h_{1\text{opt}}$  and at 5 mT,

TABLE I. A summary of the NMR spectral fitting for the untreated Co powder.

Site	Rel. int. ( $\pm 3\%$ )	Observed frequency ( $\pm 0.2$ MHz)	Observed FWHM <sup>a</sup> ( $\pm 0.2$ MHz)	Literature FWHM <sup>a,b,c</sup> (MHz)	Literature frequency <sup>b,c</sup> (MHz)
fcc	20	212.9	1.7	0.5	213.1
hcp	52	220.9	1.1	0.8	221.0
hcp deformation fault <sup>d</sup>	10	214.2/215.6	0.7/1.3	1.1/0.5	214.0/215.5
fcc deformation fault <sup>e</sup>	19	217.1/218.9	2.3/1.7	0.5/1.5	217.0/219.0

<sup>a</sup>FWHM=full width half maximum.

<sup>b</sup>Reference 7.

<sup>c</sup>Reference 15.

<sup>d</sup>A fcc twin fault or observed locally in NMR as two hcp deformation faults.

<sup>e</sup>A hcp twin fault or observed locally in NMR as two fcc deformation faults.

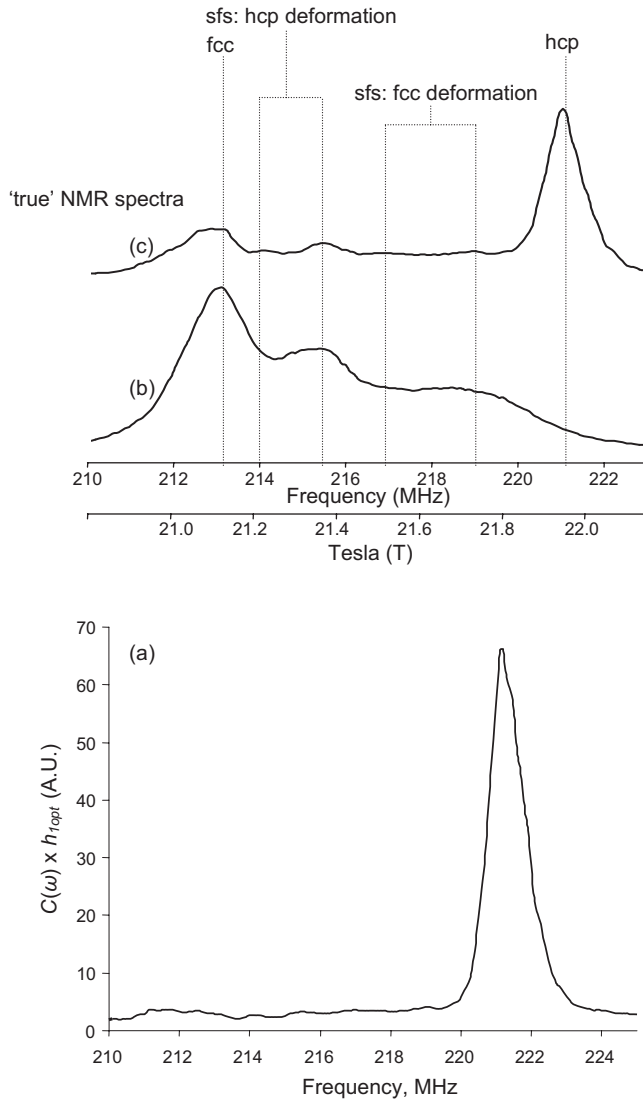


FIG. 4. (a) The dimensionless frequency-dependent conversion factor,  $C(\omega) \times h_{1\text{opt}}$ , between the spectra taken when  $h_1 = 5$  mT and the corrected NMR intensity. (b) The observed <sup>59</sup>Co NMR spectra taken of CC200 when  $h_1 = 5$  mT. (c) The corrected <sup>59</sup>Co NMR spectra of CC200, which is the product of the observed spectra when  $h_1 = 5$  mT and the dimensionless frequency-dependent conversion factor,  $C(\omega) \times h_{1\text{opt}}$ . The vertical dotted lines show the positions of the different Co sites.

and then by the dimensionless number proportional to  $h_{1\text{opt}}$ . Figure 4 shows in detail how the process works. The “raw” <sup>59</sup>Co NMR spectrum of a CC200 Co sample was acquired at  $h_1 = 5$  mT [Fig. 4(b)]. Measurements were taken at  $h_{1\text{opt}}$  for each site to confirm that multiplying by  $C(\omega)$  was giving correct spin-echo intensities. The correction factors working at  $h_1 = 5$  mT are  $\sim 2$ –70 for different frequencies [Fig. 4(a)]. As is clear from the figure, the “true” NMR spectrum [Fig. 4(c)] is quite different compared to that acquired at  $h_1 = 5$  mT. Thus correction of the directly observed spectral intensity is necessary to provide quantitatively the most accurate site-specific information. It could be asked: why not work at an rf field nearer to the maximum of the major sites, say,  $\sim 100$  mT rather than 5 mT so that the correction would

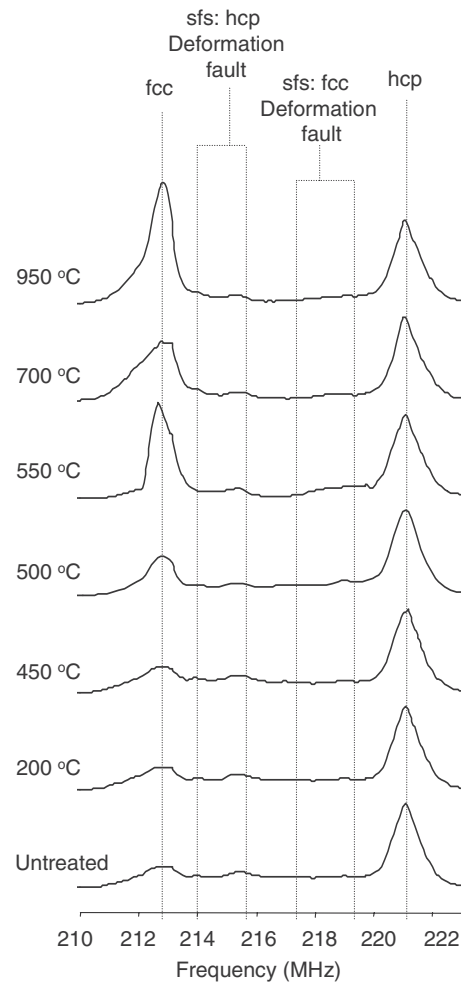


FIG. 5. Corrected <sup>59</sup>Co NMR spectra of Co powders with various treatment temperatures. All spectra are normalized to the hcp resonance at 221.0 MHz. The vertical dotted lines show the positions of the different Co sites.

be less marked? This would indeed be preferred *if* it were not for the penalty paid in signal to noise. To generate such high rf a 4-mm-diameter probe was used which significantly decreases the amount of sample, and hence the time to get the necessary signal to noise over the entire 10 MHz becomes prohibitively long to make it a practical widely used probe. Hence the philosophy adopted here was to deduce the correction factor once with high accuracy, and then subsequently get excellent signal to noise using a much larger sample and then correct this. Other approaches could be used but this investigation suggests that this is the most practical approach to encourage widespread use of the technique.

Figure 5 displays the corrected <sup>59</sup>Co NMR spectra for all CC samples with different treatment temperatures. For comparison, all spectra are normalized to the hcp resonance at 221.0 MHz. The effect of the treatment temperatures on the individual Co sites is clear. Spectra were fitted with Gaussian lines for quantitative analysis, with the results summarized in Table II. Figure 6 shows the relative intensity of the overall faulted (all sfs) and unfaulted (fcc and hcp) phases. No appreciable change was observed for faulted and unfaulted phases between room temperature and 500 °C; however,

TABLE II. A summary of spectral fitting for samples with different treatment temperatures.

Sample <sup>a</sup>	Unfaulted		Faulted			
	fcc	hcp	sfs: hcp deformation fault <sup>c</sup>		sfs: fcc deformation fault <sup>d</sup>	
	213.1 MHz (±3%) <sup>b</sup>	221.0 MHz (±3%)	214.0 MHz (±3%)	215.5 MHz (±3%)	217.0 MHz (±3%)	219.0 MHz (±3%)
Untreated	20	52	2	8	12	7
CC200	22	50	2	9	11	6
CC450	24	48	2	9	11	6
CC500	25	48	2	5	10	10
CC550	39	43	2	4	1	11
CC700	48	43	1	3	1	4
CC950	49	40	2	3	1	5

<sup>a</sup>The number is the temperature in degrees Celsius, e.g., CC200 is a sample heated to 200 °C and then crash-cooled.

<sup>b</sup>The errors quoted refer to the errors deduced from the reproducibility of the fits from data that has undergone processing using the procedure described in the text, starting from the different sets of raw data.

<sup>c</sup>A fcc twin fault or, as observed locally in NMR, two hcp deformation faults.

<sup>d</sup>A hcp twin fault or, as observed locally in NMR, two fcc deformation faults.

from 500 to 550 °C, a sudden increase in the unfaulted phases (~10%) and an accompanying decrease in the faulted phases were observed. This suggests that the overall faulted heating

→ unfaulted phase transformation occurs at  $500 \pm 25$  °C. Sfs are produced when the Co metal is put under stress and/or when the phase transformation between hcp and fcc occurs.<sup>34</sup> Thus at temperatures above the phase-transition temperature, the Co atoms are in the favorable unfaulted fcc phase, and when samples are quenched by the CC treatment, the Co atoms are “locked” into this unfaulted fcc phase, leaving fewer Co nuclei in the faulted phase.

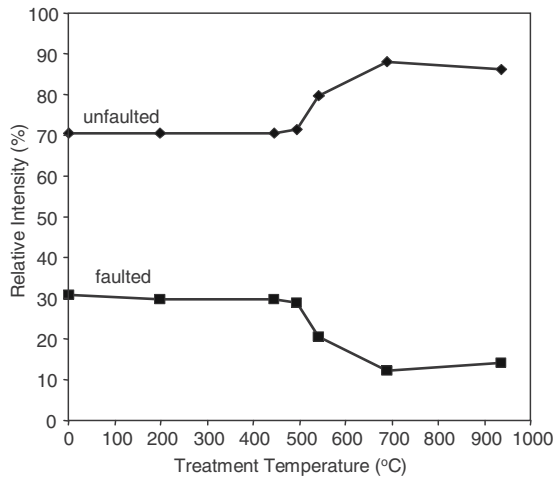


FIG. 6. A plot of relative intensity of faulted (all sfs) and unfaulted (fcc and hcp) Co sites as a function of treatment temperature. The representation of symbols is as follows: unfaulted phase (diamonds); faulted phase (square).

**B. hcp→fcc allotropic phase transformation**

In bulk Co materials, it is reported that the hcp phase is dominant below the phase-transition temperature of 417 °C, with the fcc phase becoming more dominant above 417 °C.<sup>1</sup> Unlike bulk Co materials, the untreated Co powder used here has an appreciable fcc phase content, approximately 20%. One would expect to observe a hcp→fcc phase transition at a certain temperature. Figure 7 shows the temperature dependence of the total hcp/fcc ratio. A hcp→fcc phase transition is clearly visible at a temperature  $\sim 500 \pm 25$  °C, where a sudden drop of hcp/fcc ratio is observed. The observed phase-transition temperature is higher than the previous reported 417 °C for bulk Co.<sup>1</sup> This can be rationalized by (1) difference in particle size: the Co crystallites in this Co pow-

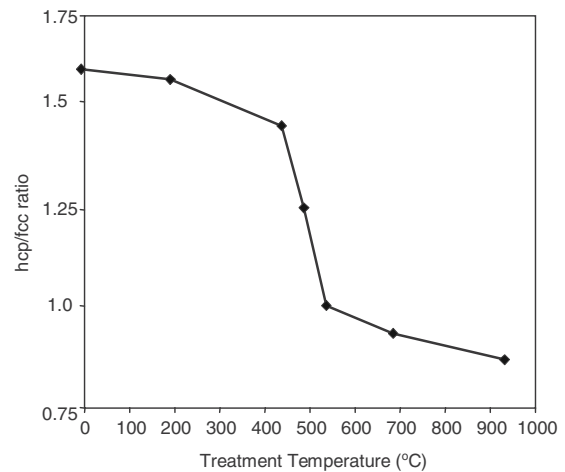


FIG. 7. A plot of hcp/fcc ratio as a function of treatment temperature. The sfs at 214 and 215 MHz are considered as hcp phase, and the faults at 217 and 219 MHz are considered as fcc phase.

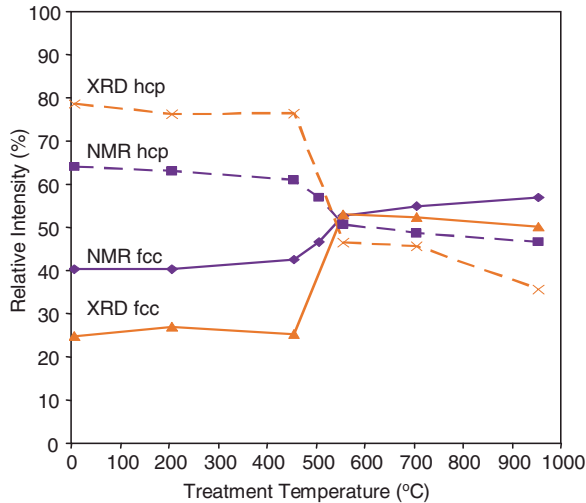


FIG. 8. (Color online) A plot of relative intensity of both hcp (dashed lines) and fcc (solid lines) phases as a function of treatment temperature taken with NMR (blue) and XRD (red). For the NMR results hcp is taken by adding the unfaulted hcp and faulted hcp phases; similarly fcc is taken by adding the unfaulted fcc and faulted fcc phases.

der are much smaller than that of bulk Co materials,<sup>5</sup> and (2) differences in the heat treatments: the measurement of hcp/fcc ratio in bulk Co in the reference was done *in situ* using XRD methods, whereas the measurements in Co powder were carried out after cooling from a treatment temperature allowing some Co to recover back to hcp phase <sup>cooling</sup> (fcc  $\rightleftharpoons$  hcp). For the same reason, a small hcp/fcc ratio of <sup>heating</sup>  $\sim 0.9$  is found for CC above 550 °C. If the NMR measurements were taken *in situ* at temperature, then one might expect that the hcp/fcc ratio would remain constant below the allotropic transition temperature with a rapid decrease to zero at the phase-transition temperature, where fcc would then become the dominant phase and no recovery of hcp would occur. However a good estimate of the phase-transition temperature can be determined from this indirect approach by analyzing the different Co sites after the sample is rapidly quenched from each heat treatment temperature.

### C. XRD vs NMR measurements

For analytical comparison, the relative intensities for fcc and hcp have been measured using both XRD and NMR methods, and the results are displayed in Fig. 8. It is important to note that the NMR intensity results for hcp is the summation of all the Co nuclei in the unfaulted hcp and in the hcp deformation faults (sfs). The figure clearly shows that both the NMR and XRD measurements resulted in the same transition temperature of  $500 \pm 25$  °C. However the relative signal intensity for hcp and fcc differs by up to 20% between the two techniques. This can be explained by the different limitations in the two methods. For the internal-field  $^{59}\text{Co}$  NMR, particles with diameter  $< 15$  nm are considered “silent.”<sup>21</sup> However the Co particles used in this study are in the micrometer regime; thus they are unlikely to

be silent in  $^{59}\text{Co}$  NMR. The potential effects of domain-wall distributions on the NMR signal also should be noted at this point. For XRD, amorphous or locally disordered regions are often difficult to observe. Consequently, the disordered Co in the sf phase cannot be reliably characterized by XRD. On the above basis,  $^{59}\text{Co}$  NMR gives more accurate quantitative information compared to XRD. For example: (1) the 30% Co faulted phase observed by NMR, from room temperature to 500 °C in Fig. 6, may explain the 15% difference in the relative intensity between NMR and XRD for data collected from samples that were heat treated between room temperature and 500 °C, shown in Fig. 8. (2) As shown in Fig. 6 the sfs reduce by  $\sim 20\%$  at heat treatment temperatures above 500 °C; a similar ( $\sim 10\%$ ) reduction in the relative intensities of different phases (hcp and fcc) is observed between XRD and NMR (see Fig. 8). Although the aim here was to characterize the different sites and phase transitions within the metallic Co, in looking more completely at the samples, the formation of the cobalt oxide phases is important. Then one benefit of XRD is the observation of the surface oxides [see Fig. 3(b)] which is impossible with internal-field  $^{59}\text{Co}$  NMR.

### V. CONCLUSIONS

The application of  $^{59}\text{Co}$  NMR spectroscopy to characterize the allotropic phase transformation of small crystallite Co has been demonstrated. The hcp  $\rightarrow$  fcc phase-transition temperature is measured *ex situ* by quantifying the amounts of hcp and fcc Co from samples after heat treatment. The phase-transition temperature is estimated to be  $500 \pm 25$  °C. It has been shown that quantitative measurements of sfs in Co can be achieved with internal-field  $^{59}\text{Co}$  NMR spectroscopy. This technique was used to show that the sf content below the allotropic phase-transition temperature is approximately constant, accounting for  $\sim 30\%$  of the Co nuclei. However heating above the phase-transition temperature reduces the sf content to  $\sim 10\text{--}20\%$  of all Co nuclei.

Both NMR and XRD have been shown to be capable of measuring the relative amounts of hcp and fcc; however the two techniques result in different absolute quantitative information. These differences are attributed to the fact that Co sites cannot be readily probed by XRD. Hence NMR produces more directly interpretable site information than XRD. The present  $^{59}\text{Co}$  NMR study clearly illustrates the potential of NMR spectroscopy on ferromagnetic materials with small particle sizes ( $< 2$   $\mu\text{m}$ ) that are highly faulted, which are difficult to accurately characterize with XRD. It is believed that the NMR approach described here does provide quantitative data on the different sites although it is more complex than for nonmagnetic materials. Even at a qualitative level this NMR approach is competitive for understanding structural problems involving cobalt in magnetic materials. There are many applications for this approach, such as, to some, key industrial scale physiochemical problems involving Co. Some examples include cobalt in electrode materials (e.g.,  $\text{LiCoO}_2$ ), as a drying agent (e.g., paints), and as a catalyst, both homogeneous and heterogeneous, in the plastic and petrochemical industries.<sup>35</sup>

## ACKNOWLEDGMENTS

R.S. thanks EPSRC-GB and Johnson Matthey for funding. A.W. thanks BBSRC and NSERC. EPSRC-GB and the University of Warwick are thanked for partial funding of NMR equipment. G. Goodlet and S. Spratt are thanked for

the electron microscopy used to confirm particle sizes as is D. Keeble for useful discussions regarding XRD results. Some of this work was started while T.J.B. was a visitor at Warwick funded by the Leverhulme Trust who is thanked for this funding.

\*Author to whom correspondence should be addressed; Present address: Department of Physics, University of Warwick, Gibbet Hill Road, Coventry CV4 7AL, United Kingdom; FAX: +44 24 7669 2016; M.E.Smith.1@warwick.ac.uk

<sup>1</sup>C. R. Houska, B. L. Averbach, and M. Cohen, *Acta Metall.* **8**, 81 (1960).

<sup>2</sup>H. L. Gaigher and N. G. van der Berg, *Electrochim. Acta* **21**, 45 (1976).

<sup>3</sup>J.-E. Bidaux, R. Schaller, and W. Benoit, *Acta Metall.* **37**, 803 (1989).

<sup>4</sup>P. Tolédano, G. Krexner, M. Prem, H. P. Weber, and V. P. Dmitriev, *Phys. Rev. B* **64**, 144104 (2001).

<sup>5</sup>O. Kitakami, H. Sato, Y. Shimada, F. Sato, and M. Tanaka, *Phys. Rev. B* **56**, 13849 (1997).

<sup>6</sup>K. J. D. MacKenzie and M. E. Smith, *Multinuclear Solid-state NMR of Inorganic Materials* (Pergamon, Amsterdam, 2002).

<sup>7</sup>A. C. Gossard and A. M. Portis, *Phys. Rev. Lett.* **3**, 164 (1959).

<sup>8</sup>A. M. Portis and R. H. Lindquist, in *Magnetism IIA*, edited by G. T. Rado and H. Suhl (Academic, New York, 1965), Chap. 6.

<sup>9</sup>E. A. Turov and M. P. Petrov, *Nuclear Magnetic Resonance in Ferro- and Antiferromagnets* (Halsted, New York, 1972).

<sup>10</sup>A. P. Guimarães, *Magnetism and Magnetic Resonance in Solids* (Wiley, New York, 1998).

<sup>11</sup>L. E. Toth and S. F. Ravitz, *J. Phys. Chem. Solids* **24**, 1203 (1963).

<sup>12</sup>M. Kawakami, T. Hihara, Y. Kōi, and T. Wakiyama, *J. Phys. Soc. Jpn.* **33**, 1591 (1972).

<sup>13</sup>H. Enokiya, *J. Phys. Soc. Jpn.* **42**, 796 (1977).

<sup>14</sup>H. Brömer and H. L. Huber, *J. Magn. Magn. Mater.* **8**, 61 (1978).

<sup>15</sup>J. Sort, S. Surinach, J. S. Muñoz, M. D. Baró, M. Wojcik, E. Jedryka, S. Nadolski, N. Sheludko, and J. Nogués, *Phys. Rev. B* **68**, 014421 (2003).

<sup>16</sup>E. A. M. van Alphen, S. G. E. te Velthuis, H. A. M. de Gronckel, K. Kopinga, and W. J. M. de Jonge, *Phys. Rev. B* **49**, 17336 (1994).

<sup>17</sup>M. Cerisier, K. Attenborough, E. Jedryka, M. Wojcik, S. Nadolski, C. Van Haesendonck, and J. P. Celis, *J. Appl. Phys.* **89**,

7083 (2001).

<sup>18</sup>A. Michel, V. Pierron-Bohnes, J. P. Jay, P. Panissod, S. Lefebvre, M. Bessière, H. E. Fischer, and G. Van Tendeloo, *Eur. Phys. J. B* **19**, 225 (2001).

<sup>19</sup>H. Wieldraaijer, W. J. M. de Jonge, and J. T. Kohlhepp, *Phys. Rev. B* **72**, 155409 (2005).

<sup>20</sup>A. N. Murty, A. A. Williams, R. T. Obermyer, and V. U. S. Rao, *J. Appl. Phys.* **61**, 4361 (1987).

<sup>21</sup>A. N. Murty, M. Seamster, A. N. Thorpe, R. T. Obermyer, and V. U. S. Rao, *J. Appl. Phys.* **67**, 5847 (1990).

<sup>22</sup>R. C. La Force, S. F. Ravitz, and G. F. Day, *Phys. Rev. Lett.* **6**, 226 (1961).

<sup>23</sup>Y. Kōi, A. Tsujimura, T. Hihara, and T. Kushida, *J. Phys. Soc. Jpn.* **17**, 96 (1962).

<sup>24</sup>P. C. Riedi and R. G. Scurlock, *J. Appl. Phys.* **39**, 1241 (1968).

<sup>25</sup>S. Nasu, H. Yasuoka, Y. Nakamura, and Y. Murakami, *Acta Metall.* **22**, 1057 (1974).

<sup>26</sup>C. Mény, E. Jędryka, and P. Panissod, *J. Phys.: Condens. Matter* **5**, 1547 (1993).

<sup>27</sup>M. Malinowska, M. Wójcik, S. Nadolski, E. Jędryka, C. Mény, P. Panissod, M. Knobel, A. D. C. Viegas, and J. E. Schmidt, *J. Magn. Magn. Mater.* **198-199**, 599 (1999).

<sup>28</sup>P. Panissod, J. P. Jay, C. Mény, M. Wojcik, and E. Jedryka, *Hyperfine Interact.* **97/98**, 75 (1996).

<sup>29</sup>D. Massiot, F. Fayon, M. Capron, I. King, S. Le Calvé, B. Alonso, J.-O. Durand, B. Bujoli, Z. Gan, and G. Hoatson, *Magn. Reson. Chem.* **40**, 70 (2002).

<sup>30</sup>T. Hyde, *Platinum Met. Rev.* **52**, 129 (2008).

<sup>31</sup>R. A. Young, *The Rietveld Method* (Oxford University Press, Oxford, 1995).

<sup>32</sup>H. E. Swanson, H. F. McMurdie, M. C. Morris, E. H. Evans, B. Paretzkin, J. H. de Groot, and S. J. Carmel, *Natl. Bur. Stand. (U.S.) Monogr.* **4**, 10 (1966).

<sup>33</sup>M. Nuding and M. Ellner, *J. Alloys Compd.* **252**, 184 (1997).

<sup>34</sup>C. Hitzenberger, H. P. Karthaler, and A. Korner, *Acta Metall.* **33**, 1293 (1985).

<sup>35</sup>J. D. Donaldson, *Cobalt in Chemistry* (Cobalt Development Institute, Guildford, UK, 1986).